Published in final edited form as:
Magn Reson Imaging. 2015 February ; 33(2): 185–193. doi:10.1016/j.mri.2014.10.009.

Quantifying Errors in Flow Measurement Using Phase Contrast Magnetic Resonance Imaging: Comparison of Several Boundary Detection Methods

Jing Jiang, MS[a,d], **Paul Kokeny, MS**[a,e], **Wang Ying, MS**[a,b], **Chris Magnano, MS**[c], **Robert Zivadinov, MD PhD**[c], and **E. Mark Haacke, PhD**[a,d,e,f]

[a]Department of Biomedical Engineering, Wayne State University, Detroit, MI, USA

[b]College of Information Science and Engineering, Northeastern University, Shenyang, Liaoning province, China

[c]Buffalo Neuroimaging Analysis Center, State University of New York, Buffalo, New York, USA

[d]Department of Radiology, Wayne State University, Detroit, Michigan, USA

[e]Magnetic Resonance Innovations, Inc., Detroit, Michigan, USA

[f]Department of Electrical and Computer Engineering, McMaster University, Hamilton, Ontario, Canada

Abstract

Quantifying flow from phase-contrast MRI (PC-MRI) data requires that the vessels of interest be segmented. This estimate of the vessel area will dictate the type and magnitude of the error sources that affect the flow measurement. These sources of errors are well understood and mathematical expressions have been derived for them in previous work. However, these expressions contain many parameters that render them difficult to use for making practical error estimates. In this work, some realistic assumptions were made that allow for the simplification of such expressions in order to make them more useful. These simplified expressions were then used to numerically simulate the effect of segmentation accuracy and provide some criteria that if met, would keep errors in flow quantification below 10% or 5%. Four different segmentation methods were used on simulated and phantom MRA data to verify the theoretical results. Numerical simulations showed that including partial volumed edge pixels in vessel segmentation provides less error than missing them. This was verified with MRA simulations, as the best performing segmentation method generally included such pixels. Further, it was found that to obtain a flow error of less than 10% (5%), the vessel should be at least 4 (5) pixels in diameter, have an SNR of at least 10:1 and a peak velocity to saturation cut-off velocity ratio of at least 5:3.

Corresponding author: E. Mark Haacke, Magnetic Resonance Innovations, Inc., 440 East Ferry Street, Detroit, MI, 48202, USA, Tel: 1-313-758-0065, Fax:1-313-758-0068, nmrimaging@aol.com.

INTRODUCTION

Quantifying blood flow is becoming an increasingly important means by which to study vascular disease with applications not only in the usual cardiovascular diseases, but also in neurovascular and neurodegenerative diseases as well [1,2]. Phase-contrast MRI (PC-MRI) is a well-established, noninvasive means by which to measure the velocity of moving spins. It allows for flexible temporal and spatial resolution and has seen use in a variety of applications in quantifying vascular function and hemodynamics within both clinical and research fields. Segmentation of the vessel lumen is an important factor in obtaining an accurate measure of flow from PC-MRI data. Manual segmentation is time consuming and, being observer-dependent, can lead to significant variations of area measurement and consequently affect the accuracy of the flow measurement [3]. This is especially a problem when working with poor resolution or slow flow rates, such as with cerebral spinal fluid in the aqueduct [4]. Automatic segmentation algorithms generally provide improved consistency and efficiency [5]. Various algorithms for automatic or semi-automatic segmentation based on full width half maximum, thresholding, active contour modeling, and dynamic programming have been proposed [5–9], yet a thorough comparison of these methods with a theoretical backing is still lacking.

This study aims to provide a practical analysis of the effects of vessel segmentation accuracy, vessel size, signal-to-noise ratio (SNR), peak blood velocity; and MR sequence parameters such as resolution, repetition time, slice thickness, and velocity encoding value (VENC) on flow quantification error. This was done using our in-house software, SPIN (Signal Processing in NMR), on both simulation and phantom data. Simple expressions to quantify these effects are also developed and validated. SPIN includes four different automatic vessel segmentation algorithms to be used for this purpose: full-width half maximum (FWHM) thresholding, histogram based thresholding [10], standard deviation based thresholding, and dynamic programming [11]. These methods are reviewed and their ability to extract average flow rate accurately from vessels with varying size relative to the in plane resolution, peak blood velocity, and SNR, are presented.

MATERIALS AND METHODS

To evaluate the robustness of the methods presented in this paper, (1) the theoretical effects of vessel segmentation on the accuracy of the flow measurement were considered, (2) simulated data for a variety of vessel diameters with different MR parameters was assessed, and (3) phantom flow data was evaluated. Human data testing will be presented separately.

There are multiple sources of error that are present in quantifying flow using PC-MRI. The noise in MR signal leads to random error in the phase image that affects quantification. When a voxel contains both moving and stationary spins, such as at the edge of a vessel, it can be shown that the phase value of that voxel does not correctly represent the average velocity present [12]. This type of error is systematic and is referred to as partial volume error. Other systematic errors include: intravoxel phase dispersion, velocity aliasing, and imaging plane misalignment. An in-depth analysis of these sources was performed in 1993 by Wolf et al [13]. Eddy currents and concomitant fields can also lead to errors in flow

quantification by creating phase that is unrelated to moving spins [14]. The focus in this paper is on the errors associated with segmentation accuracy, which can be explained by partial volume error, vessel size, and SNR; consequently, other systematic errors were not included in this analysis. We also only focus on standard Cartesian acquisition schemes, as it has been shown that performing PC imaging using echo planar imaging create additional sources of error [15].

Theoretical Effects of Vessel Segmentation Accuracy on Flow Quantification

The vessel boundary resulting from any segmentation method will be either “oversized”, “undersized”, or “midsized”. An oversized boundary is defined as one that contains at least all pixels that include any amount of vessel. An undersized boundary contains only pixels that consist entirely of vessel. A midsized boundary will contain some, but not all, pixels that contain part vessel. The type of boundary will dictate what sources of error will be present in flow quantification.

Flow error from an oversized boundary

Flow calculated from an oversized boundary will suffer from partial volume error. Making some practical assumptions about flow and signal behavior, the general expression for this error [13] can be simplified to estimate the worst possible flow error from partial volume effects as a function of the scaled vessel diameter, λ (defined as vessel diameter in units of pixels). The simplified expression is given by

$$\frac{\varepsilon_{PV}}{F_V} \approx -\frac{0.55\kappa(3\lambda - 1.4)^2}{\lambda^3(\lambda^2 + 1.5\kappa\lambda - 0.69\kappa)} \quad (1)$$

where

$$\kappa = \left[\frac{2\Delta S \nu_p}{3S_t(TH/TR)}\right] \quad (2)$$

ε_{PV} is the difference between measured and true flow, F_V, TH is the slice thickness, TR is the repetition time, ΔS is the difference in between the maximum signal within the vessel lumen and signal of the surrounding tissue, S_t, and ν_p is the peak velocity.

The assumptions made in order to simplify the general expression include an isotropic in-plane resolution of 1mm, laminar blood flow, and a constant partial volume fraction (ratio of moving spins to total spins present in an edge pixel) of 0.7, which was found to represent a worst-case scenario. Time of flight behavior was included in this simplification by assuming that the signal from blood decreases linearly with velocity when below what will be referred to as the “saturation cut-off velocity”, defined as *TH* /*TR*, and is a constant when above this cut-off. This cut-off arises from the concept of fully unsaturated blood moving into the imaging slice before each RF excitation [16]. When below the cut-off, the same volume of blood may get excited numerous times and thus provide less signal. A more thorough explanation of the derivation of Equation 1 is given in Appendix A.

Flow error from an undersized boundary

For an undersized boundary, there will be no partial volume effects and the error will result from missing velocity data from the vessel. Let λ_B represent the diameter, in pixels, of a segmented area of a vessel with laminar flow and true diameter, λ, in pixels. Given that the segmented area is undersized, it must follow that $\lambda_B < \lambda$. The flow within this area, F_B, is given as

$$F_B = \frac{\pi}{4} \nu_p \left({\lambda_B}^2 - \frac{{\lambda_B}^4}{2\lambda^2} \right) \quad (3)$$

and the relative error from an undersized boundary is given by

$$\frac{F_V - F_B}{F_V} = - \frac{\left({\lambda_B}^2 - \lambda^2 \right)^2}{\lambda^4} \quad (4)$$

The segmentation algorithms used in this study are applied to the magnitude images. Thus the outcome of being over- or under-sized will depend on λ and SNR throughout the vessel lumen.

Effects of SNR

Flow quantification from all boundary types will be affected by noise. A general expression for the variance of flow measurements was derived by Wolf et al [13]; however, it is difficult to obtain any practical results from the expression in its initially given form. Part B of the appendix shows the steps taken in order to reformulate the expression in terms of standard deviation, σ_F, relative to F_V and as a function of λ, λ_B, SNR, VENC (ν_e), and peak velocity, ν_p. The appropriate expressions will be different for over- and under-sized boundaries and are given as

$$\frac{\sigma_F}{F_V} = \frac{4\sqrt{2}}{\sqrt{\pi^3}} \left(\frac{\nu_e}{\nu_p} \right) \left(\frac{1}{SNR} \right) \left(\frac{\lambda_B}{\lambda^2} \right) for \lambda_B \geq \lambda \quad (5)$$

$$\frac{\sigma_F}{F_V} = \frac{4\sqrt{2}}{\sqrt{\pi^3}} \left(\frac{\nu_e}{\nu_p} \right) \left(\frac{1}{SNR} \right) \left(\frac{1}{\lambda_B} \right) for \lambda_B < \lambda \quad (6)$$

It is seen that the error of the flow measurement from noise is inversely proportional to SNR and λ (or λ_B for an undersized boundary).

Numerical Analysis

In reality, segmented vessels will only contain a discrete number of pixels. Thus, there will be different continuous ranges of λ that will result in the same discrete number of pixels that contain vessel only. To take this into account, a numerical simulation can be performed that includes a distinction between intra-lumen pixels and partial volumed edge pixels. This also allows for calculation of true partial volume fraction and thus a more accurate error calculation using equation A10 in the appendix rather than assuming a “worst-case” value of

0.7 for partial volume fraction as was done in deriving Equation 1. Including all pixels that contain only vessel would represent the best possible undersized boundary, while further including pixels with any signal from the vessel would represent the best possible oversized boundary (see Figures 1A, 1B). The undersized boundary error was calculated from Equation 4, estimating λ_B by assuming the number of inside pixels to be its corresponding area. This numerically simulated comparison was performed on a vessel centered on a pixel with a peak velocity of 20cm/sec (see Figure 1C).

It is seen that including the partial volumed pixels in the estimation of the vessel size will result in less error than missing these pixels. Overestimation greater than shown in Figure 1B increases the amount of noise included and also risks greater influence of background phase variations throughout the cardiac cycle. However, such an overestimation can be easily avoided through visual observation of the segmentation result. Based on this theoretical estimate and numerical simulation, it is seen that it is better to overestimate vessel area than to underestimate when performing flow quantification.

Simulation of blood flow with vessels of different diameters

A cine phase contrast scan was simulated for 25 time-points over a complete cardiac cycle (one frame of which is seen in Figure 2). The image contained ten vessels, each with a distinct laminar velocity profile based on vessel sizes and profiles from neck flow measurements in human subjects as illustrated in Figure 3. Vessels 2 and 4 will be subject to phase aliasing since a VENC of 50cm/sec, which is recommended for the measurement of internal carotid arteries and jugular veins [17], was chosen for this simulation. SPIN automatically corrects for aliasing, which was verified by observing the time profiles of the maximum positive and negative velocity of vessels 2 and 4.

The images were created on an ultrahigh resolution grid (4096×4096) and cropped in k-space to provide a desired resolution in the image domain. Pixel intensities were calculated using a saturation cut-off velocity of both 6cm/sec and 12cm/sec, which are in the range of values typically seen in flow studies. For velocities above this cut-off, a magnitude signal intensity value of 500 was used. Otherwise, to mimic TOF effects, the intensities were modeled to decrease linearly with velocity, approaching the surrounding tissue signal intensity of 150 when the velocity reaches 0. These signal intensities values were chosen from measuring ten PC MRI normal control datasets. The simulation was created for three different resolutions: a matrix size of 256×256 corresponding to $\Delta x = 1$mm; a matrix size of 512×512 corresponding to $\Delta x = 0.5$mm; and a matrix size of 1024×1024 corresponding to $\Delta x = 0.25$mm providing vessel diameters ranging from 2 to 32 pixels.

Different levels of noise were added to each resolution providing vessel SNR of ∞ (no noise), 20:1, 15:1, and 10:1. This was accomplished using a Monte Carlo simulation to add a set of zero-mean Gaussian distributed numbers to the real and imaginary part of the k-space data. The standard deviation of these sets were calculated based on a maximum vessel lumen intensity of 500. Different simulation seed points were used for each slice.

Phantom experiments

To verify results from simulations and numerical analysis, a series of steady flow experiments on a 3T MR scanner (Verio, Siemens Healthcare, Erlangen, Germany) was performed.

A digital injector (Solaris, MEDRAD INC., Warrendale, Pennsylvania, USA) was used to specify a flow rate within a 3mm diameter tube ($\lambda \approx 10$) and was imaged multiple times using various flow rates and VENC values. The SNR of these images was roughly 10:1. Figure 4A shows a photograph of the phantom along with acquired magnitude (Figure 4B) and phase (Figure 4C) images. Only objects 1 and 2 were processed due to their perpendicular alignment to the image acquisition plane. The phantom was scanned using a gradient echo sequence with the following parameters: TE = 10ms, TR = 95ms, in-plane resolution = $0.28\times0.28mm^2$, TH = 4mm, FA = 20°, and FOV=$128\times128mm^2$. Flow rates of 0.1mL/sec (with Venc = 4 and 5cm/sec), 0.2mL/sec (with Venc = 8, 10, and 15cm/sec), 0.5mL/sec (with Venc = 20 and 25cm/sec), and 1mL/sec (with Venc = 40, 50, and 60cm/sec) were used.

Vessel Segmentation Algorithms

In post-processing, four different region growing algorithms were tested on each data set by applying them to each vessel separately in the magnitude image of the first time point and copying the resulting boundary to the rest of the time points. A description of each algorithm follows.

a) *Full Width Half Maximum Threshold (FWHM)*: The 25 pixels with the highest intensities are chosen from within a user defined square pixel area centered at a seed point (where the user clicks) that surrounds a vessel. (This area is referred to as the “search box” and it can have an area bigger than 25 pixels but this area must cover the vessel. If the vessel is too small, the data can be interpolated.) The mean of these 25 pixels is calculated as representing the maximum intensity inside the vessel. Half of that value is used as the threshold intensity. Points whose intensities are higher than the threshold and satisfy connectivity to the seed point are marked as the selected vessel.

b) *Dynamic Programming (DP)*: An initial vessel boundary is obtained using the FWHM method. The DP algorithm [11] is then run for a series of rays connecting each boundary point to the center of the vessel. This algorithm adjusts the original boundary points by maximizing signal derivative change and minimizing curvature change. A more detailed description can be found in [11].

c) *Histogram Threshold (HT)*: The histogram of all values in the search box is calculated to acquire an assumed bi-modal histogram of two signals (flowing blood and surrounding tissue). A cost calculation based on Otsu segmentation [10] is used to separate these two distributions and run iteratively until an optimal separation value to differentiate the two signals is decided as the threshold value.

d) *Standard Deviation Threshold (SD)*: The HT method is used first to find the optimal separation value in the magnitude image between the flowing blood and surrounding tissue. The mean and standard deviation of all intensities below that optimal separation value in the same search box described in FWHM method (assumed to represent surrounding tissue) is calculated. This mean plus two times the standard deviation from those points is then used as the new threshold value.

Each method can be used in a 2D or 2D/1D mode (i.e., including all time points throughout the cardiac cycle). The 2D mode segments a vessel from a single slice where the resulting boundary can then be copied to all other time points, whereas the 2D/1D mode segments a vessel for all time points automatically in order to compensate for any vessel movement throughout the cardiac cycle. In this study, the 2D mode was used for all segmentations. SPIN does allow the user to manually adjust boundaries on individual time points in case a vessel changes shape or moves during the cardiac cycle, but since the simulations and phantoms had consistent areas throughout the dataset, this feature was not used. It is also suggested that a region containing no flow (NFA) is drawn on the stationary tissue, near the areas of interest in order to correct for any remnant non-zero background phase variation that may exist. This step was performed for the phantom datasets.

RESULTS

Numerical Analysis

The percentage error in flow for the numerically simulated data as a function of λ is shown in Figure 1C. It reveals a stair step like behavior due to pixel discretization where, at certain values of λ, the number of pixels that contain only vessel suddenly jumps. Despite this local anomalous pixel quantification behavior, generally, as λ increases, the error decreases. A similar but less dramatic effect can be seen in the oversized boundary case. For $\lambda > 5$ in Figure 1C, the error drops below 5% and by $\lambda \geq 10$, it has fallen below 2% (compared to roughly 5% for the undersized boundary case). This agree with the findings from Merkx et al based on FWHM in uCT [5].

Simulation

The next stage was to test the flow quantification accuracy of the segmentation methods in a simulated MRA experiment without noise over a range of vessel sizes. The SD threshold method never resulted in an undersized boundary. In this case, for a vessel diameter greater than or equal to 5 pixels, flow error was less than 5% (Figure 5A). The FWHM method performed the best out of the remaining three with an error less than roughly 5% for most λ. DP performed better than HT, though both had errors greater than 10% even for larger λ. For vessel diameters less than 4 pixels, flow error showed an exponential-like increase (up to 40%), independent of segmentation method. These points were not included in the plot. The gap in λ values between 12 and 14 pixels was due to our choices of simulated vessel sizes and resolutions. Plotting the flow error as a function of percent area error (Figure 5B), it can be seen that the SD method consistently overestimated the area and does generally the best in estimating flow. The other methods tend to underestimate the flow with a flow error

approaching zero as the error in area decreases (due to increasing λ). Partial volume errors resulting from the SD segmentation boundaries were found to be in agreement with Equation A10 (Figure 6), which suggests that the SD method is an optimal segmentation method and λ greater than 4 can achieve acceptable accuracy. The FWHM method could theoretically be altered to use less than half-maximum to lower the intensity threshold for region growing and result in a larger boundary; however, to choose an optimal percentage of maximum would require knowledge of the vessel signal, tissue signal, and noise. Using this information would essentially mimic the SD method.

In addition to λ and the segmentation method, the peak velocity also plays an important role as it dictates the signal within the vessel. To test the role of peak velocity, the SD segmentation method was used in the 10:1 SNR simulations for both a saturation cut-off velocity of 6 cm/sec and 12 cm/sec. The resulting boundaries associated with the peak velocity were copied to the rest of the time points. Figure 7 shows a scatter plot of error versus peak velocity for $\lambda \geq 8$ pixels. Smaller vessels were influenced by other sources of error and could not isolate this effect. It was found that for vessels at least 8 pixels in diameter, a peak velocity to saturation cut-off velocity ratio of at least 5:3 was needed to keep flow error below 10%.

As expected, adding noise to the simulations degraded the performance of all the region growing algorithms. The SD method still continued to perform the best, resulting in a flow error of less than 5% for most vessel diameters greater than or equal to 5 pixels (Figure 8). The FWHM performed the second best again, and the DP method seemed to be more affected by noise than the other methods, as it performed worse than the HT method at all noise levels.

Phantom

Over all combinations of flow rates and VENC values used in the phantom, the SD method resulted in an average error of 5.7%, FWHM resulted in an average error of −5.1%, HT resulted in an average of error of −7.6%, and DP resulted in an average error of −19.9%. The superior performance of the SD method matches our simulation results.

DISCUSSION

The flow errors analyzed in this study arise from noise, partial volume effects and vessel voxel selection for the area determination. The extent of the error from these sources is dependent on both vessel size (in pixels) and the size of the boundary created. The individual boundary determination methods are affected by SNR, peak velocity and saturation cut-off velocity.

Vessel diameter in pixels is perhaps the most important factor. For the no noise cases and a vessel diameter of less than 5 pixels, the predicted error from partial volume alone is above 5%. Quantifying flow from vessels smaller than 4 pixels is simply not reliable no matter how good the vessel boundary is. Thus, it is important to use a resolution that will ensure that any vessels of interest will have a λ of at least 4 to 5 pixels in the image (4 if 10% error would be acceptable or 5 if 5% error is the goal).

With a large enough vessel diameter, the factor that impacted flow error the most was the accuracy of the boundary. An undersized boundary can be detrimental to flow quantification accuracy even for large vessels. A best-case undersized boundary can lead to flow error of over 5% even for vessel diameters up to 11 pixels. The accuracy of the vessel segmentation depends on the algorithms used, while the performance of these algorithms depends on SNR, peak velocity, and saturation cut-off velocity.

The results show that the SD method generates the least error due to the fact that it tends to not underestimate the size of the vessel. The FWHM and HT methods performed similarly while the DP method tended to underestimate the size of the vessel more frequently. Since the performance of the DP method is affected by other intrinsic parameters, it may be possible to adjust for improved results. However, these parameters were not tested in this study.

Noise affects flow error in two ways. First, noise introduces random error into the phase image, as described in Equations 5 and 6. Secondly, noise affects the performance of the segmentation algorithms. Even with less desirable parameters such as a vessel size of at least 5 pixels, SNR of 10:1, peak velocity of 7cm/sec, and 25 time points, the error described in Equation 5 was found to be negligible (<3%) compared to the error from the segmentation algorithm performance. This finding agrees with a study in which quantification accuracy from 3T and 1.5T scanners were compared [18]. Increasing noise tended to shift the error towards more negative values. This trend can be understood two different ways. The first is that as the SNR decreases, the standard deviation of the background tissue increases, resulting in a higher threshold and smaller boundary. The same concept applies to the FWHM method since the highest intensity pixels will likely increase. The second is that as the noise increases, the lower signal from the edge of the vessel will be more difficult to differentiate from the background. However, for the SD segmentation method, the error in flow remained on the order of 5% even for an SNR of 10:1 (see Figure 8C).

The peak velocity and saturation cut-off velocity are important as well. Even with a large λ, a low peak velocity in the vessel relative to the saturation cut-off velocity can reduce the vessel lumen signal in the magnitude images (and hence the SNR). From the post-processing point of view, choosing a time point where the peak velocity is high, such as during systole, to perform segmentation should generate a better result. Lowering the saturation cut-off velocity can help compensate for low peak velocities, but would either require reducing the slice thickness or increasing the repetition time, though this can be problematic; for example, decreasing slice thickness will decrease SNR, while increasing TR lengthens the scan time. This illustrates a tradeoff between imaging parameters, which would need to take into account the application.

Practically, the flow error from the phantom was higher than expected given that the diameter of the vessels analyzed was close to 10 pixels. This could be attributed to inaccuracy of the estimate of the actual flow as well as inadequate compensation of background phase variability [17,19]. Integrating all this information together is the key to a successful measurement of flow in the human body. A rule of thumb that can be ascertained from all the materials discussed herein is that the user should choose an SNR of 10:1 or

higher, a λ of 4 or higher, and the SD boundary detection method to ensure that the error in flow is less than 10% (5% or lower). Higher resolution, while improving accuracy, also leads to longer scan times. Today, at 3T, it is not uncommon to image with an in-plane resolution of 0.5mm, a smaller slice thickness of 2.5mm for higher resolution, a repetition time of 20ms (leading to a saturation cut-off velocity of 12.5cm/sec), a Venc of 50cm/sec to 100cm/sec and still have an SNR in the vessels of 20:1. From this one can estimate the changes in SNR as resolution increases; doubling resolution is a viable option, reducing the SNR by a factor of 2 if the read bandwidth is kept constant. This suggests that faster imaging methods that might reduce SNR or increasing in-plane resolution to 0.25mm to image small vessels should be possible. However, for most of the major vessels in the neck, a resolution of 0.5mm should suffice to allow for flow errors of less than 5 to 10% of λ of 5 and 4, respectively. Future work will deal with imaging flow in the major vessels in the neck at 3T.

CONCLUSION

Obtaining accurate flow measurements requires an excellent estimate of the boundary of the vessel and sufficient SNR in the magnitude image. The results presented here suggest that to obtain a flow error of less than 10% (5%) requires a vessel that is 4 (5) or more pixels in diameter, an SNR of 10% or greater, and a ratio of peak speed over saturation cut-off velocity of 5:3 or higher. The best performing method for estimating the boundary of a vessel appears to be the SD method based on a modified histogram approach.

ACKNOWLEDGMENTS

Research reported in this publication was supported by the National Heart, Lung, And Blood Institute of the National Institutes of Health under Award Number R42HL112580. The content is solely the responsibility of the authors and does not necessarily represent the official views of the National Institutes of Health.

We are also thankful to Paul Polak and Michael G. Dwyer for critical review of the paper.

REFERENCES

1. Feng W, Utriainen D, Trifan G, Sethi S, Hubbard D, Haacke EM. Quantitative flow measurements in the internal jugular veins of multiple sclerosis patients using magnetic resonance imaging. Rev Recent Clin Trials. 2012; 7(2):117–126. [PubMed: 22356242]
2. Haacke EM, Feng W, Utriainen D, et al. Patients with multiple sclerosis with structural venous abnormalities on MR imaging exhibit an abnormal flow distribution of the internal jugular veins. J Vasc Interv Radiol. 2012; 23(1):60–68. e61–e63. [PubMed: 22221473]
3. Hoogeveen RM, Bakker CJ, Viergever MA. Limits to the accuracy of vessel diameter measurement in MR angiography. J Magn Reson Imaging. 1998; 8(6):1228–1235. [PubMed: 9848733]
4. Wahlin A, Ambarki K, Hauksson J, Birgander R, Malm J, Eklund A. Phase contrast MRI quantification of pulsatile volumes of brain arteries, veins, and cerebrospinal fluids compartments: repeatability and physiological interactions. J Magn Reson Imaging. 2012; 35(5):1055–1062. [PubMed: 22170792]
5. Merkx MA, Bescos JO, Geerts L, Bosboom EM, van de Vosse FN, Breeuwer M. Accuracy and precision of vessel area assessment: Manual versus automatic lumen delineation based on full-width at half-maximum. J Magn Reson Imaging. 2012; 36(5):1186–1193. [PubMed: 22826150]
6. Kozerke S, Botnar R, Oyre S, Scheidegger MB, Pedersen EM, Boesiger P. Automatic vessel segmentation using active contours in cine phase contrast flow measurements. J Magn Reson Imaging. 1999; 10(1):41–51. [PubMed: 10398976]

7. Oyre S, Ringgaard S, Kozerke S, et al. Accurate noninvasive quantitation of blood flow, cross-sectional lumen vessel area and wall shear stress by three-dimensional paraboloid modeling of magnetic resonance imaging velocity data. J Am Coll Cardiol. 1998; 32(1):128–134. [PubMed: 9669260]
8. Oelhafen M, Schwitter J, Kozerke S, Luechinger R, Boesiger P. Assessing arterial blood flow and vessel area variations using real-time zonal phase-contrast MRI. J Magn Reson Imaging. 2006; 23(3):422–429. [PubMed: 16463327]
9. Stalder AF, Russe MF, Frydrychowicz A, Bock J, Hennig J, Markl M. Quantitative 2D and 3D phase contrast MRI: optimized analysis of blood flow and vessel wall parameters. Magn Reson Med. 2008; 60(5):1218–1231. [PubMed: 18956416]
10. Otsu N. A Threshold Selectiom Method from Gray-Level Histograms. IEEE Transactions on Systems, Man, and Cybernetics. 1979; 9:5.
11. Jiang J, Haacke EM, Dong M. Dependence of vessel area accuracy and precision as a function of MR imaging parameters and boundary detection algorithm. J Magn Reson Imaging. 2007; 25(6): 1226–1234. [PubMed: 17520741]
12. Tang C, Blatter DD, Parker DL. Accuracy of phase-contrast flow measurements in the presence of partial-volume effects. J Magn Reson Imaging. 1993; 3(2):377–385. [PubMed: 8448400]
13. Wolf RL, Ehman RL, Riederer SJ, Rossman PJ. Analysis of systematic and random error in MR volumetric flow measurements. Magn Reson Med. 1993; 30(1):82–91. [PubMed: 8371679]
14. Kilner PJ, Gatehouse PD, Firmin DN. Flow measurement by magnetic resonance: a unique asset worth optimising. J Cardiovasc Magn Reson. 2007; 9(4):723–728. [PubMed: 17613655]
15. Moser KW, Georgiadis JG, Buckius RO. On the accuracy of EPI-based phase contrast velocimetry. Magnetic resonance imaging. 2000; 18(9):1115–1123. [PubMed: 11118766]
16. Brown, RW.; Cheng, Y-CN.; Haacke, EM.; Thompson, MR.; Venkatesan, R. Magnetic resonance imaging : physical principles and sequence design. Hoboken, New Jersey: John Wiley & Sons, Inc.; 2014.
17. Walker PG, Cranney GB, Scheidegger MB, Waseleski G, Pohost GM, Yoganathan AP. Semiautomated method for noise reduction and background phase error correction in MR phase velocity data. J Magn Reson Imaging. 1993; 3(3):521–530. [PubMed: 8324312]
18. Lotz J, Doker R, Noeske R, et al. In vitro validation of phase-contrast flow measurements at 3 T in comparison to 1.5 T: precision, accuracy, and signal-to-noise ratios. J Magn Reson Imaging. 2005; 21(5):604–610. [PubMed: 15834905]
19. Lankhaar JW, Hofman MB, Marcus JT, Zwanenburg JJ, Faes TJ, Vonk-Noordegraaf A. Correction of phase offset errors in main pulmonary artery flow quantification. J Magn Reson Imaging. 2005; 22(1):73–79. [PubMed: 15971181]

APPENDIX A

Deriving worst-case flow error from partial volume as a function of lambda

Partial volume error, as derived by Wolf, can be approximated by

$$\varepsilon_{PV} \cong 2\pi(f\Delta x)^2\nu_p\left[\frac{g}{1+f(g-1)}-1\right][1-\frac{2f}{3\lambda}] \quad (7)$$

where f is the fraction of moving spins in a voxel, Δx is the in-plane resolution, ν_p is the peak velocity of the assumed laminar profile, g is the ratio of the magnitude signal from moving and stationary isochromats within a voxel, and λ is the diameter of the vessel in units of pixels.

If the velocity of blood flow in a vessel is less than the saturation cut-off of the slice thickness divided by the repetition time, *TH* /*TR*, the in-flow effect starts to diminish and the

magnitude signal will decrease. At the edge of the vessel with laminar flow, the velocity will approach zero and the signal from blood will become saturated. Figure A1a shows a general plot of signal as a function of velocity. Assuming that the signals of static blood and tissue are equal, which is a reasonable assumption as the T1 values of blood and muscle are similar, the value of *g* will approach 1 at the edges of a vessel, greatly reducing error. Since the magnitude signal of the moving spins behaves deterministically, *g* can be written as a function of *f* according to the 1-D model of an edge pixel shown in figure A1b, which assumes that all velocities in the edge pixel are below the saturation cut-off velocity.

In this 1D model, the fraction of moving spins in the edge voxel, *f*, is seen to be

$$f=\lambda/2-\lambda/2 \quad (8)$$

where the lower tailed bracket represents the floor function, returning the largest integer not greater than value within it. The signal from the stationary tissue is a constant, S_t, and the signal of the moving spins, S_v, is a function of distance in pixels, $S(q)$. The average value of the magnitude signal from the moving spins in this pixel can be calculated by

$$\overline{S_\nu}=\frac{1}{\lambda/2-\lambda/2}\int_{\lambda/2}^{\lambda/2} S(q)dq \quad (9)$$

The signal will reach a maximum, S_M, when velocity is above *TH /TR* and will be assumed to decrease proportionally with velocity until at the edge of the vessel where it will become S_t, as shown in the model. An expression for this signal can be written as

$$S(q)=\frac{\Delta S}{TH/TR}\nu(q)+S_t \nu<TH/TR \quad (10)$$

Where $\Delta S = S_M - S_t$ and $\nu(q)$ represents a laminar flow profile,

$$\nu(q)=\nu_p\left[1-4\left(\frac{q}{\lambda}\right)^2\right] \quad (11)$$

Performing the integral and division in Equation A3 gives

$$\overline{S_\nu}=S_t\left[1+\kappa\frac{\left\{3\lambda^2-4\left[(\lambda/2)^2+(\lambda/2)\lambda/2+\lambda/2^2\right]\right\}}{2\lambda^2}\right] \quad (12)$$

where

$$\kappa=\frac{2\Delta \mathrm{Sv_p}}{3\mathrm{S_t(TH/TR)}} \quad (13)$$

Combining the λ terms and factoring gives

$$\overline{S_\nu} = S_t \left[1 - 2\kappa \frac{(\lambda/2 - \lambda/2)(\lambda/2 + \lambda)}{\lambda^2}\right] \quad (14)$$

The floor function terms can be eliminated using the definition of *f*. Dividing this by S_t gives *g*.

$$g = 1 - \kappa \left[\frac{2f^2 - 3\lambda f}{\lambda^2}\right] \quad (15)$$

Normalizing Equation A1 to the true flow will result in a percentage error. The true flow, F_V, through a vessel is simply area multiplied by average velocity. For a laminar flow profile, this comes out to be $(1/8)v_p\pi\lambda^2$. Making this normalization and the substitution for *g* gives

$$\frac{\varepsilon_{PV}}{F_V} = -\frac{16\kappa\Delta x^2 f^3 (f-1)(2f-3\lambda)^2}{3\lambda^3(\lambda^2 + 3\kappa\lambda f^2 - 2\kappa f^3)} \quad (16)$$

This formula is not very useful expressed this way, so making additional simplifications is helpful. The partial volume fraction value of *f* will not be the same for all of the edge voxels around a vessel. We used Mathematica software to analyze the partial derivative of Equation A10 with respect to *f* for different practical values of λ and κ and found that *f* values between 0.65 and 0.75 provided maximum error. In an actual application, since λ will not be precisely known, it will be best to estimate a worst-case error using a value of 0.7 for *f*. An additional simplification can be made from the fact that partial volume error will increase with decreasing resolution. A resolution of 1mm is typical for velocity encoded PC-MRI experiments, and improved resolution will further reduce this error. Making these substitutions, $f = 0.7$ and $\Delta x = 1mm$, gives

$$\frac{\varepsilon_{PV}}{F_V} \approx -\frac{0.55\kappa(3\lambda - 1.4)^2}{\lambda^3(\lambda^2 + 1.5\kappa\lambda - 0.69\kappa)} \quad (A11)$$

The behavior of this function is dominated by the higher order λ terms. A value for κ can be estimated from images, giving partial volume error as a function of λ.

APPENDIX B

Deriving flow error as a function of SNR and lambda from flow variance

The variance of a flow measurement, σ_F^2, from a subtracted velocity encoded phase image can be described by the following equation from [1]:

$$\sigma_F^2 = 2\left[\frac{\nu_e}{\pi}\right]^2 \left[\frac{1}{Cp(TH)}\right]^2 \left[\frac{\pi}{4}\left(\frac{D}{\Delta x}\right)^2 + N_O\right] \quad (B1)$$

Where v_e is the encoding velocity that corresponds to a phase value of π, *C* is a coefficient of proportionality for SNR, *p* is the spin density of the voxel, *TH* is the slice thickness, *D* is vessel diameter, and N_O is the number of ROI voxels that contain no vessel. It is seen here that the variance in flow measurement actually increases with $D/\Delta x$; however, the true value for flow increases as well. Thus, like the other sources of error analyzed, it is important to normalize to the true value. The coefficient of variation, defined as the standard deviation divided by the mean, is an appropriate measure for this. The true value for flow is used to represent the mean (though it is true that systematic error will cause the actual mean to deviate from the true value). Starting with variance over the square of the true value, it can be shown that

$$\left(\frac{\sigma_F}{F_V}\right)^2=\frac{32}{\pi^3}\left(\frac{\nu_e}{\nu_p}\right)^2\left(\frac{1}{Cp(TH)}\right)^2\left[\left(\frac{1}{D\Delta x}\right)^2+\frac{4}{\pi}\left(\frac{N_O}{D^4}\right)\right] \quad \text{(B2)}$$

Given an oversized boundary with diameter, λ_B since signal to noise ratio, $SNR = Cp\,(TH)\,(\Delta x)^2$, $\lambda = D/\Delta x$, and $N_O=\left(\frac{\pi}{4}\right)(\lambda_B{}^2-\lambda^2)$ this can be rewritten as

$$\left(\frac{\sigma_F}{F_V}\right)^2=\frac{32}{\pi^3}\left(\frac{\nu_e}{\nu_p}\right)^2\left(\frac{1}{SNR}\right)^2\left(\frac{\lambda_B}{\lambda^2}\right)^2 \quad \text{(B3)}$$

And the coefficient of variation is then

$$\frac{\sigma_F}{F_V}=\frac{4\sqrt{2}}{\sqrt{\pi^3}}\left(\frac{\nu_e}{\nu_p}\right)\left(\frac{1}{SNR}\right)\left(\frac{\lambda_B}{\lambda^2}\right) \quad \text{(B4)}$$

When $\lambda_B < \lambda$, we simply set $\lambda = \lambda_B$ and obtain

$$\frac{\sigma_F}{F_V}=\frac{4\sqrt{2}}{\sqrt{\pi^3}}\left(\frac{\nu_e}{\nu_p}\right)\left(\frac{1}{SNR}\right)\left(\frac{1}{\lambda_B}\right) \quad \text{(B5)}$$

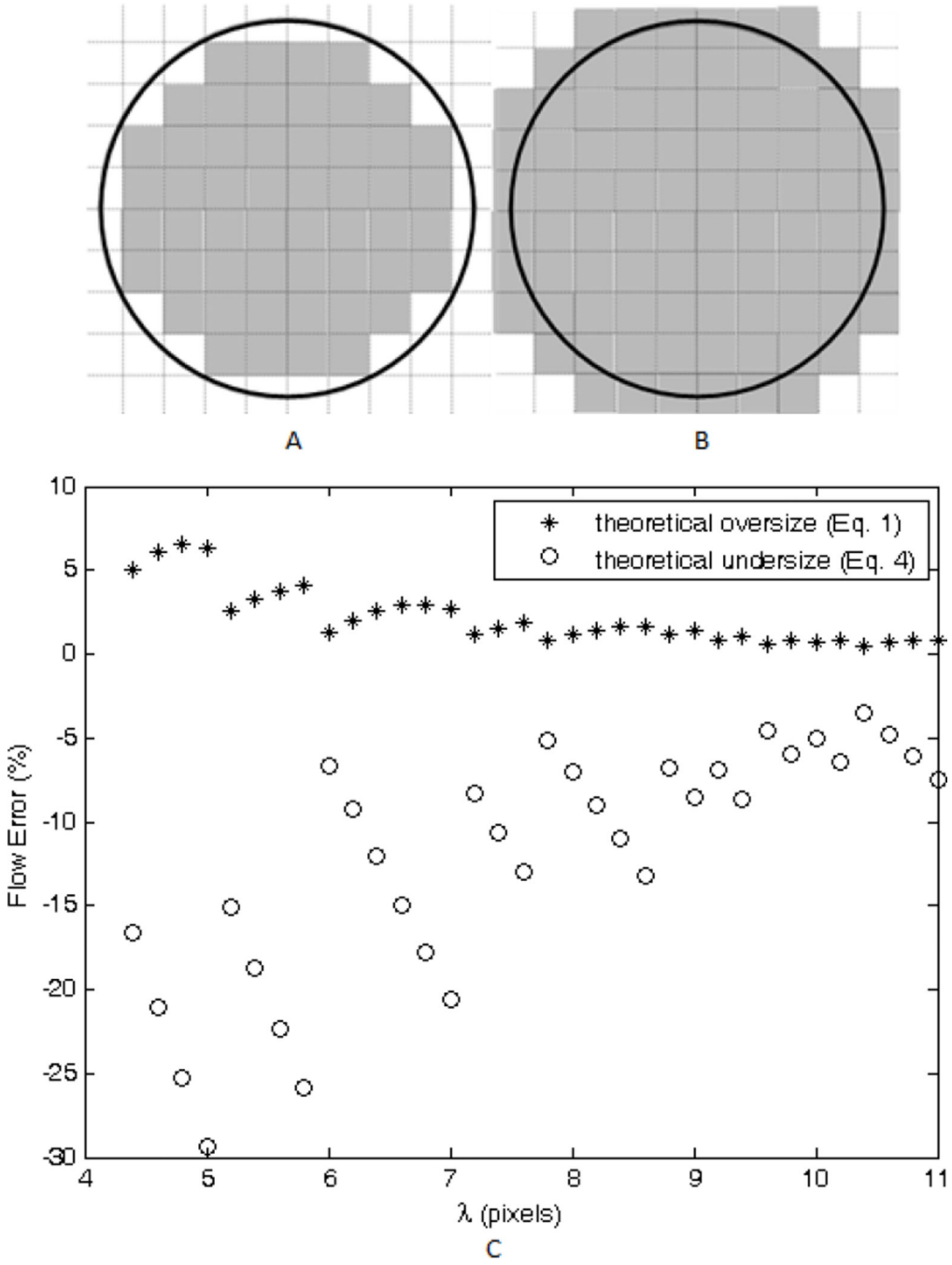

Figure 1.

Diagrams of pixel inclusion for (A) the best possible undersized boundary and (B) the best possible oversized boundary for an arbitrary vessel. The plot in (C) shows the resulting flow error as a function of vessel diameter for both boundary types in the absence of noise. The jumps in error seen are caused by the sudden inclusion of pixels as vessel diameter increases.

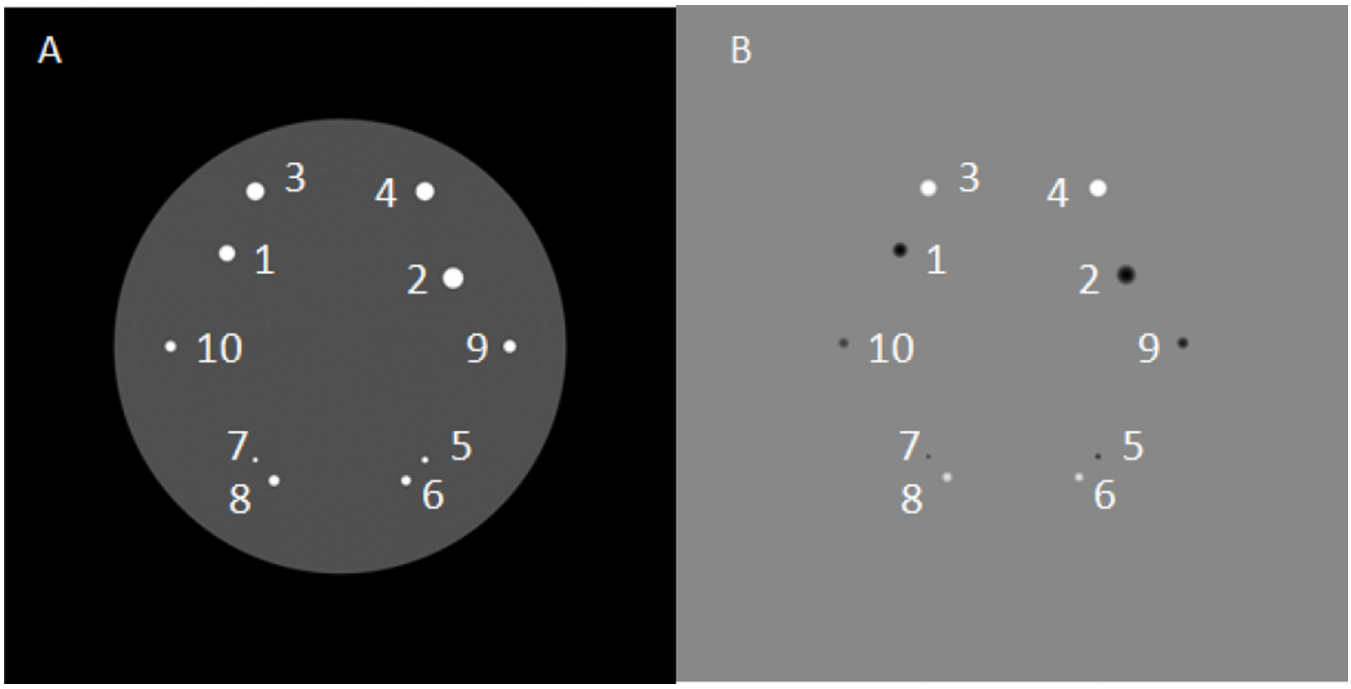

Figure 2.
(A) Magnitude and (B) phase simulated images with no noise. Each simulated vessel is labeled from 1 through 10.

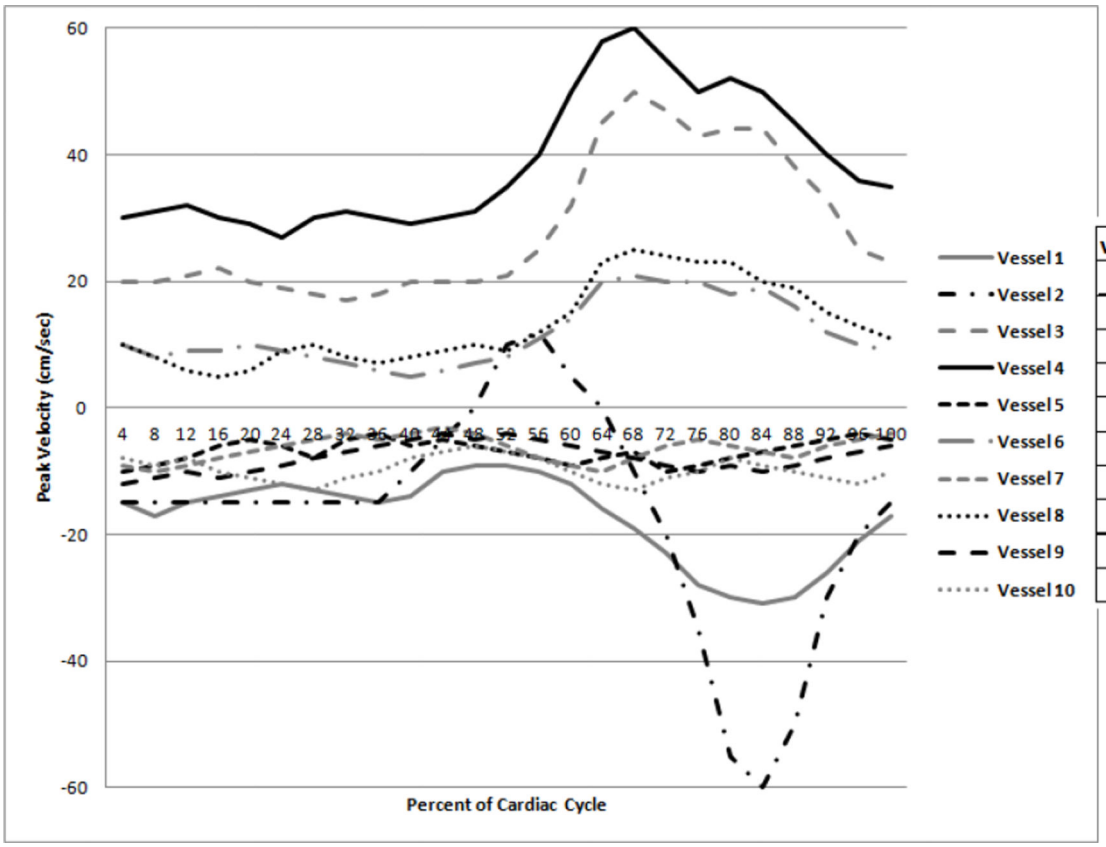

vessel	diameter (mm)
1	6.4
2	8.2
3	7.0
4	7.0
5	2.6
6	4.0
7	2.0
8	4.4
9	5.0
10	4.6

Figure 3.

Peak velocity of each simulated vessel as a function of percentage of the cardiac cycle. The numbered vessels are shown in Figure 2 and their diameters are given in the adjacent table.

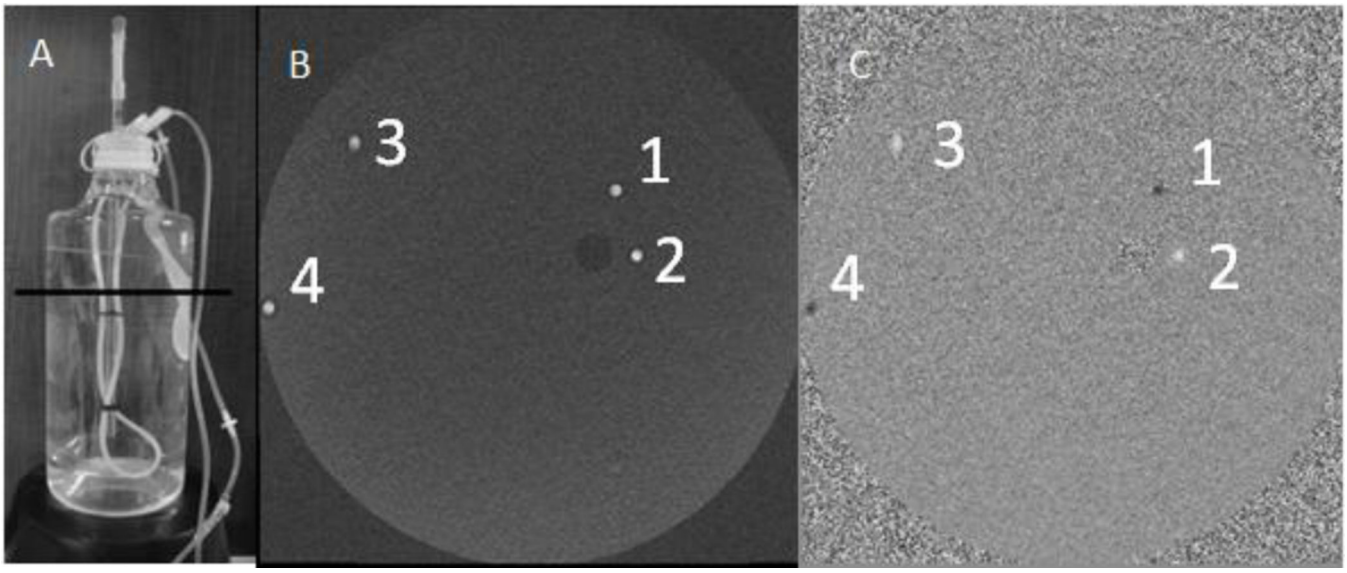

Figure 4.
Photograph of the phantom imaged on the 3T scanner (A) along with resulting (B) magnitude and (C) phase images.

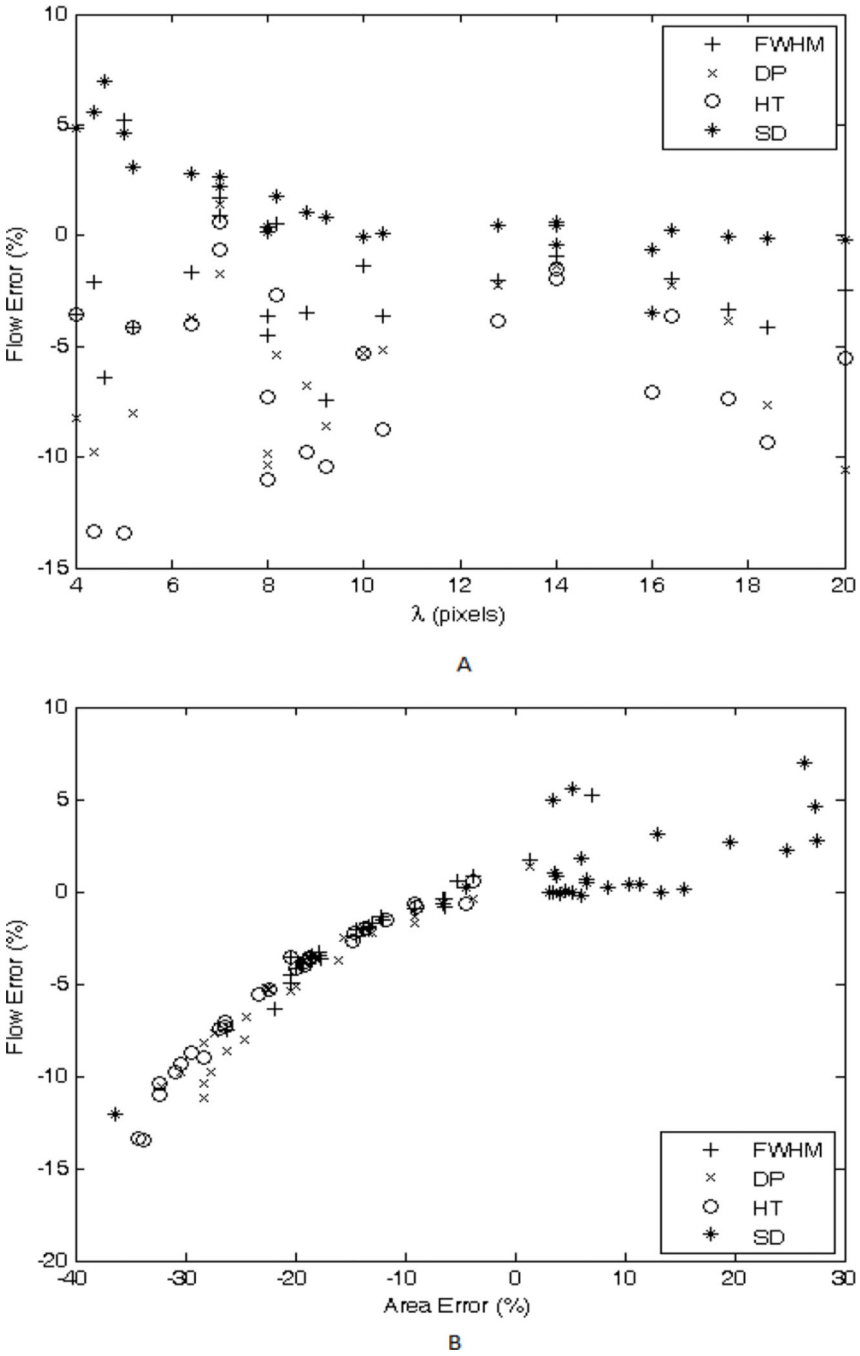

Figure 5.

Results from the no-noise simulations. (A) shows the resulting flow error from the different segmentation methods versus vessel diameter and (B) shows percent flow error versus percent area error.

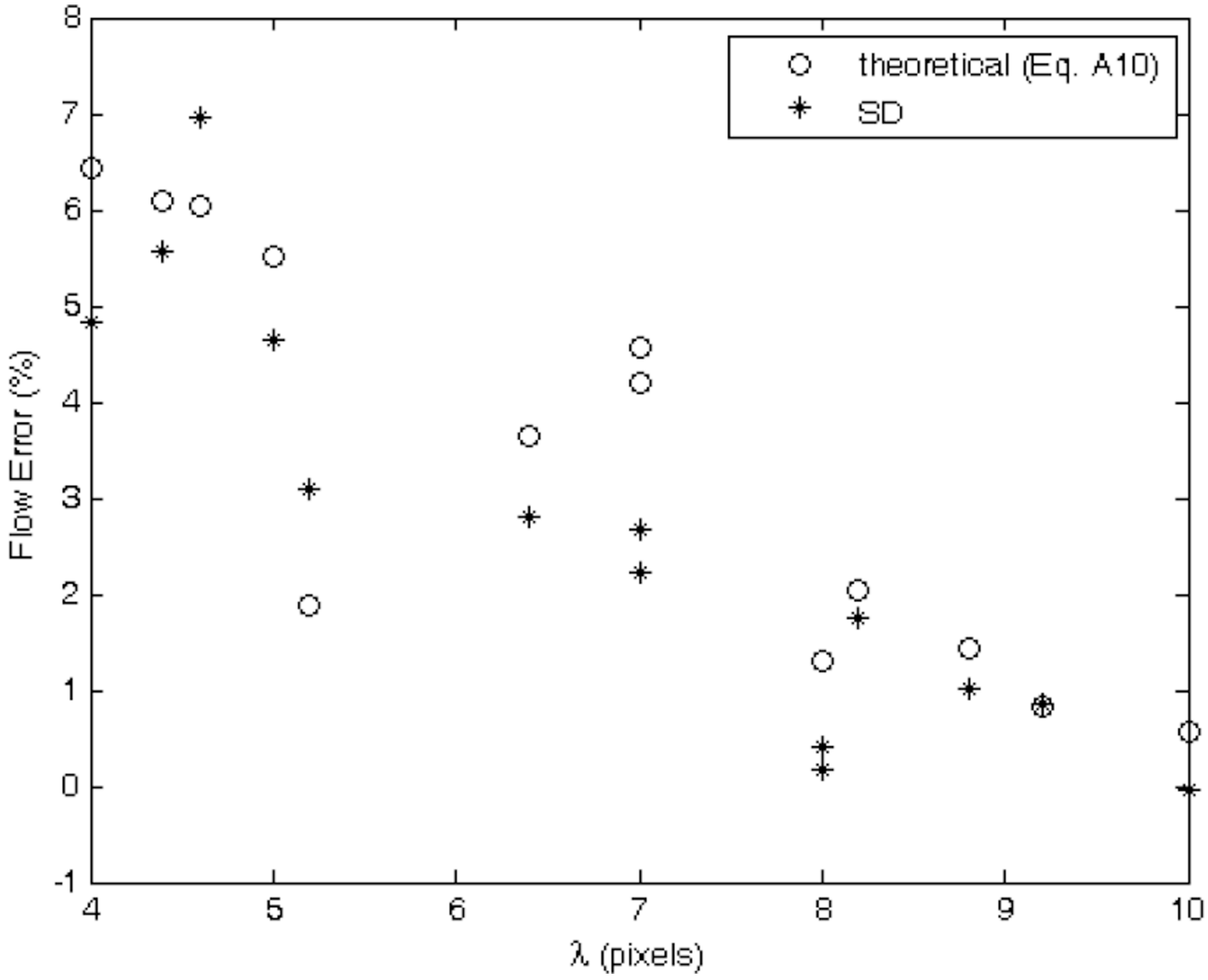

Figure 6.

A scatter plot of the results from the no-noise simulations showing percent flow error as a function of vessel diameter for both theoretical partial volume error and actual error from the SD method. These points come from all the vessels with diameters from 4 to 10 pixels with a variety of peak velocities for the 6 cm/sec saturation cut-off velocity case.

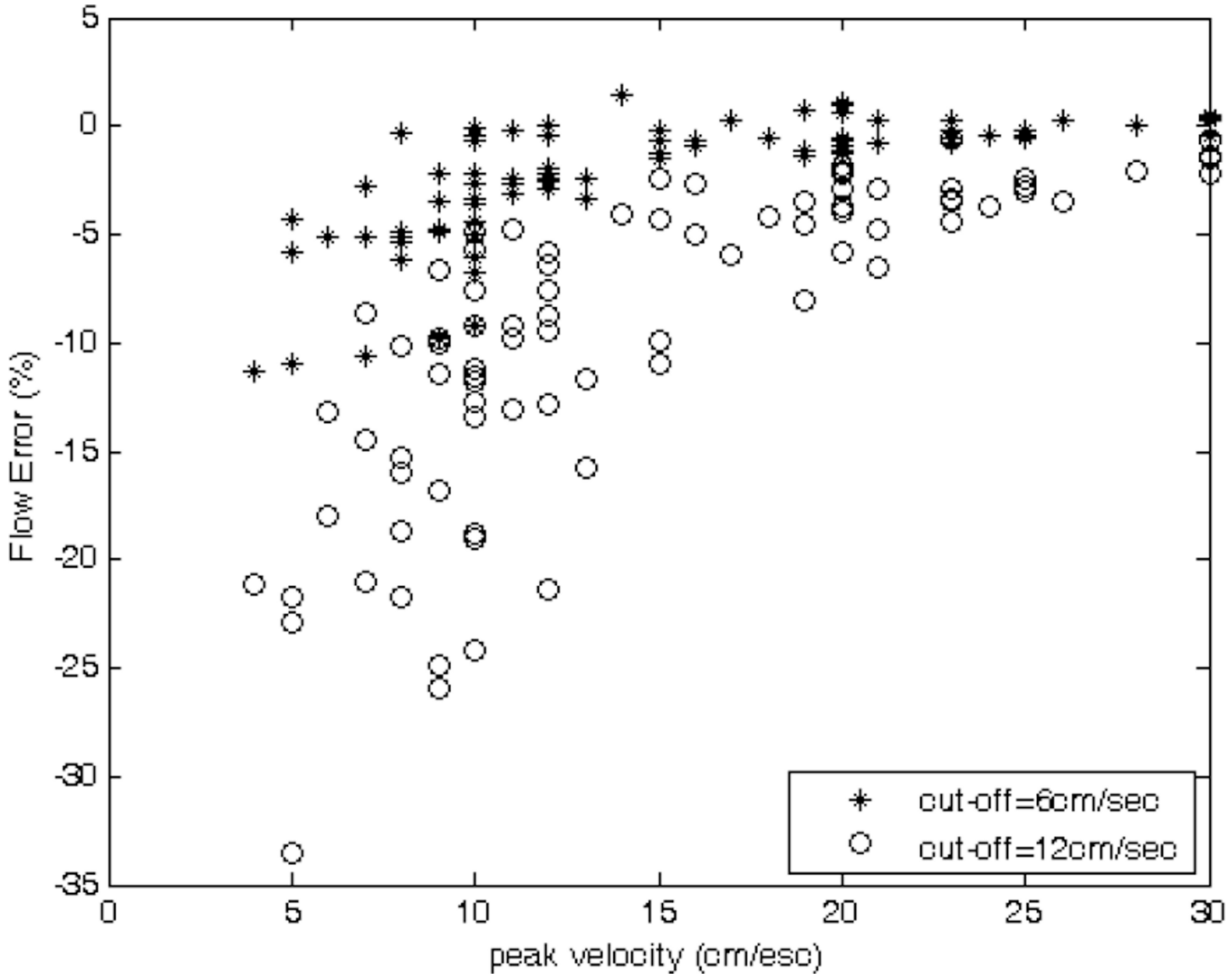

Figure 7.

A scatter plot of the results from the 10:1 SNR simulations created using two different saturation cut-off velocities and using the SD segmentation algorithm at multiple time points for all vessels greater than or equal 8 pixels in diameter. The percent flow error is plotted against the peak velocity that was present when the algorithm was run.

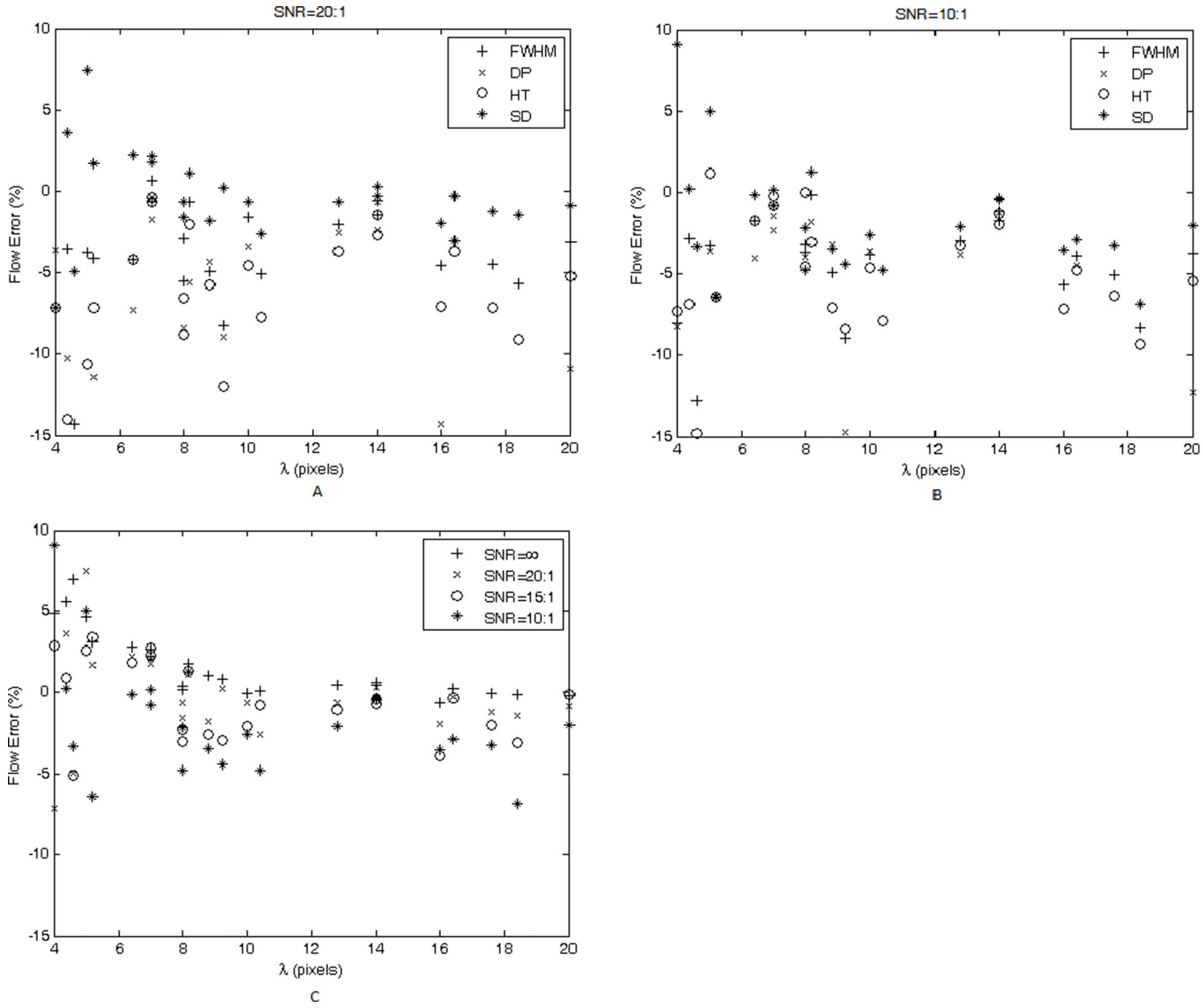

Figure 8.

Scatter plots of the results from the simulation with (A) SNR=20:1 and (B) SNR=10:1 showing percent flow error as a function of vessel diameter for all 4 segmentation algorithms. Both SNR values show a similar error which suggests that an SNR of even 10:1 can still provide good flow measurements. (C) shows results from the SD method only at different SNR values.

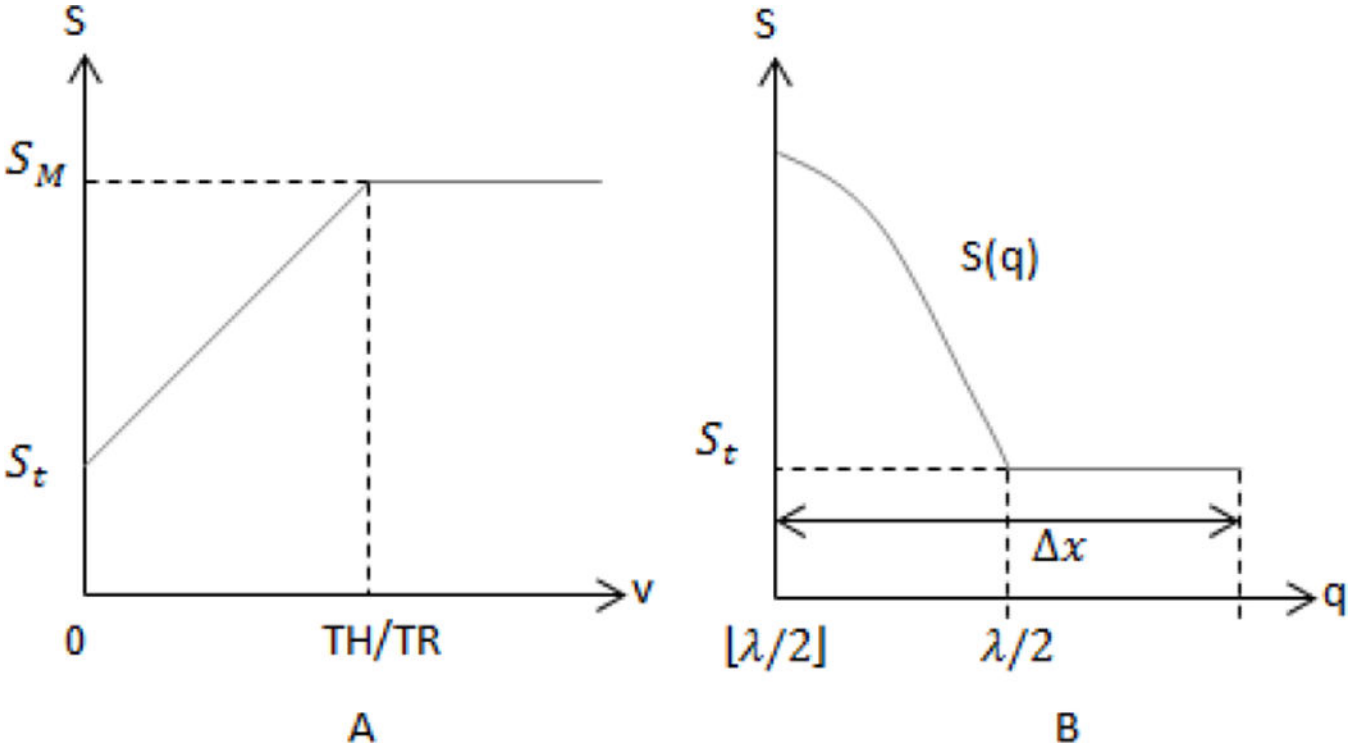

Figure A1.
A plot of magnitude signal as a function of (A) velocity and (B) distance within an edge pixel, representing the 1D model used for simplification.